nature geoscience

ARTICLES

PUBLISHED ONLINE: 14 MARCH 2010 | DOI: 10.1038/NGEO812

Zonally asymmetric response of the Southern Ocean mixed-layer depth to the Southern Annular Mode

J. B. Sallée[1]*, K. G. Speer[2] and S. R. Rintoul[1]

Interactions between the atmosphere and ocean are mediated by the mixed layer at the ocean surface. The depth of this layer is determined by wind forcing and heating from the atmosphere. Variations in mixed-layer depth affect the rate of exchange between the atmosphere and deeper ocean, the capacity of the ocean to store heat and carbon and the availability of light and nutrients to support the growth of phytoplankton. However, the response of the Southern Ocean mixed layer to changes in the atmosphere is not well known. Here we analyse temperature and salinity data from Argo profiling floats to show that the Southern Annular Mode (SAM), the dominant mode of atmospheric variability in the Southern Hemisphere, leads to large-scale anomalies in mixed-layer depth that are zonally asymmetric. From a simple heat budget of the mixed layer we conclude that meridional winds associated with departures of the SAM from zonal symmetry cause anomalies in heat flux that can, in turn, explain the observed changes of mixed-layer depth and sea surface temperature. Our results suggest that changes in the SAM, including recent and projected trends attributed to human activity, drive variations in Southern Ocean mixed-layer depth, with consequences for air–sea exchange, ocean sequestration of heat and carbon, and biological productivity.

The Southern Annular Mode (SAM) refers to an oscillation of atmospheric mass that results in changes in the westerly winds over the Southern Ocean. The positive phase of the SAM is associated with a poleward shift and strengthening of the westerlies[1]. On timescales from a few weeks to years, the SAM is the dominant mode of variability of the Southern-Hemisphere atmosphere. A tendency towards an increasingly positive SAM in recent decades is one of the strongest climate trends observed in the Southern Hemisphere. The trend has been attributed to loss of ozone in the polar stratosphere resulting from human activities[2]. Climate models predict that increases in greenhouse-gas forcing will cause a similar strengthening of the westerlies[3,4].

The influence of the SAM is manifest in many variables, including sea-level pressure, surface air temperature and geopotential height[1]. In the ocean, the SAM has been related to variability in sea ice, eddy kinetic energy, sea surface temperature (SST) and circulation[5–12]. Changes in the upper ocean associated with SAM forcing have an impact on carbon uptake and storage in the Southern Ocean, both directly, through upwelling and outgassing[13], and indirectly, by influencing nutrient cycles and phytoplankton activity[14,15].

Changes in the mixed-layer depth (MLD) have significant implications for both physical and biogeochemical processes. Correlations between horizontal velocity and variations in the MLD result in an exchange of fluid between the mixed layer and the ocean interior (that is, subduction)[16]. Intermediate waters subducted in the Southern Ocean ventilate the thermocline of the Southern-Hemisphere subtropical gyres and contribute to global budgets of heat, fresh water and nutrients[17–20]. Most of the anthropogenic carbon stored by the Southern-Hemisphere oceans has accumulated in the intermediate waters whose properties are set in the mixed layer of the Southern Ocean[21]. Anomalies in MLD modulate the exchange of oxygen and carbon dioxide between the ocean and the atmosphere[14,15]. The depth and the properties of the mixed layer also influence the availability of light and nutrients to support phytoplankton growth and therefore the overall level of biological productivity in the sea[22].

The depth and properties of the mixed layer are influenced by mechanical stirring by the wind stress and by buoyancy forcing: buoyancy loss drives convection and entrainment of underlying fluid; buoyancy gain restratifies the water column and inhibits entrainment. The mixed layer would therefore be expected to respond to changes in the atmosphere associated with climate variability and change, including the SAM and greenhouse warming. However, the response of the ocean mixed layer to changes in atmospheric forcing has not been measured owing to a lack of long-term observations in the remote Southern Ocean. The Argo programme now provides more than seven years of temperature and salinity profiles, allowing a better understanding of the dynamics and variability of the mixed layer[16,23]. Here we use the Argo profiles to relate variability in the MLD to the SAM, providing the first strong evidence of the influence of climate variability on the stratification of the upper layer of the Southern Ocean.

Variability of the Southern Ocean mixed layer

Argo floats drift with the ocean currents and measure a vertical profile of temperature and salinity in the upper 2,000 m every ten days. The floats have already provided more profiles than the historical ship-based data set. We can now resolve the large-scale structure and seasonal cycle of the MLD in the Southern Ocean (Fig. 1). Summer MLDs reach about 100 m in the vicinity of the Antarctic Circumpolar Current (ACC). Winter cooling destabilizes the water column and increases the MLD. The deepest winter mixed layers (and largest seasonal cycles) are found north of the ACC, particularly in the eastern Indian and Pacific oceans. Removal of buoyancy during autumn and winter gradually deepens the mixed

[1]CSIRO-CMAR/CAWCR, Castray Esplanade, Hobart 7000, Tasmania, Australia, [2]Oceanography, Florida State University, 900 Call St, Tallahassee, Florida 32306, USA. *e-mail: jbsallee@gmail.com.

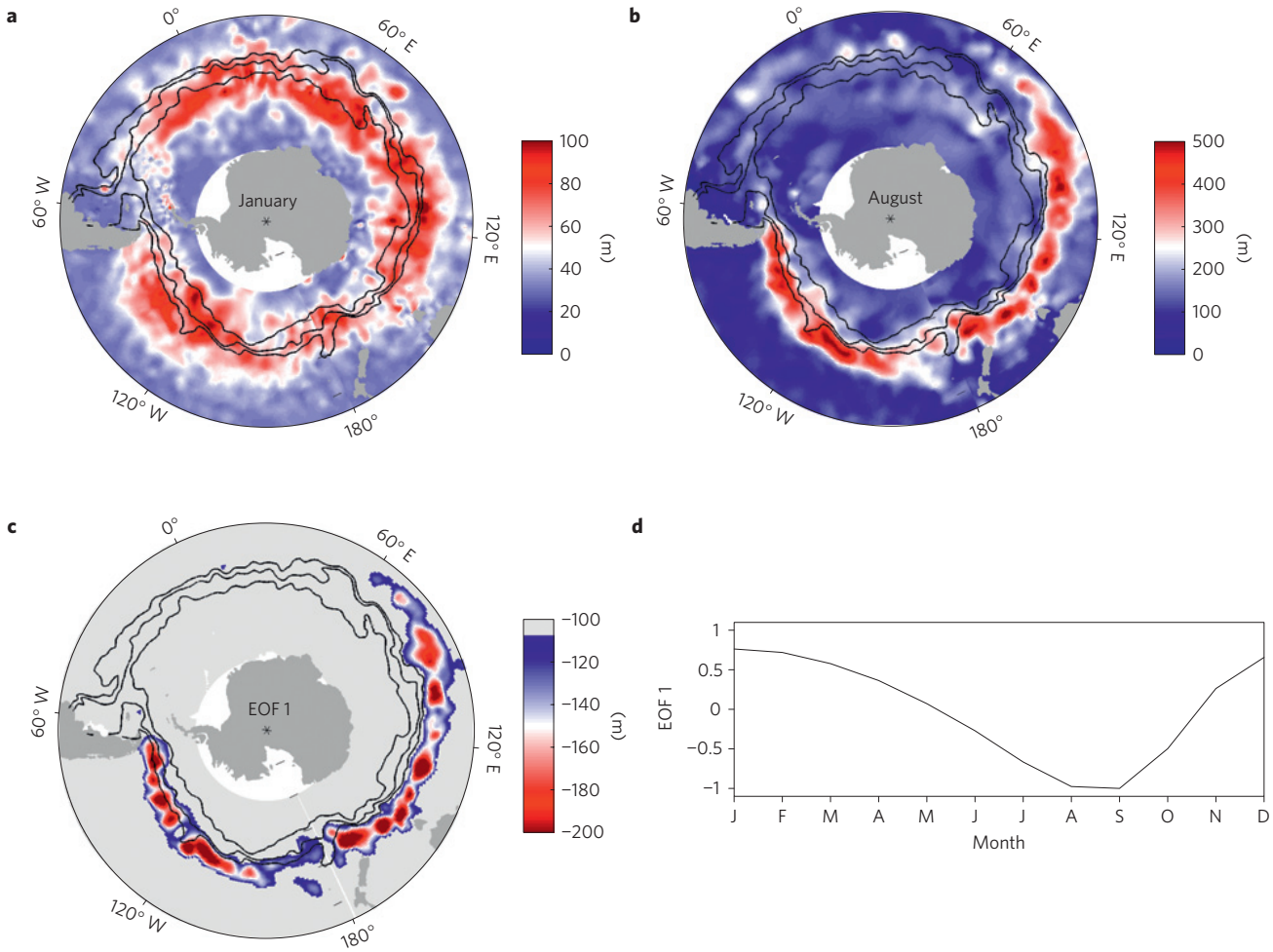

Figure 1 | Seasonal cycle of MLD. a,**b**, Summer (January) (**a**) and winter (August) (**b**) mean depth of the Southern Ocean mixed layer. **c**,**d**, First empirical orthogonal function (EOF 1) mode showing the seasonal cycle (88% of the total variance). The asterisk represents the geographic South Pole.

layer between January and September, before warming during spring and early summer rapidly re-establishes the shallow summer mixed layer. The amplitude of the seasonal cycle exceeds 400 m in some locations north of the ACC.

The intraseasonal and interannual variability of MLD about this large seasonal cycle is substantial, with values exceeding several hundred metres and a standard deviation for the whole Southern Ocean (35°–65°S) of 20 m in summer and 60 m in winter. The Argo time series is too short to allow a direct estimate of the influence of low-frequency climate variability on MLD. However, the response of the mixed layer to variations in forcing on shorter timescales can provide physical insight into the dynamical processes linking MLD changes to changes in forcing. Here we relate MLD anomalies to a monthly index of the SAM to investigate this relationship.

Composites of MLD anomalies during positive and negative events of the SAM show a clear spatial pattern, suggesting marked variability in the MLD: an average of ±100 m during positive or negative SAM events (Fig. 2c,d). We find a strongly non-zonal pattern: the MLD anomaly during positive SAM events shows a roughly wave-3 pattern, with a deepening over the eastern Indian Ocean (100°–140° E) and the central Pacific Ocean (100°–140° W) and a shallowing of the mixed layer in the western Pacific Ocean (140° E–140° W). A direct SAM–MLD relationship is supported by the negative SAM composite, which shows an opposite response of the MLD (Fig. 2d). We note that the SAM during the Argo period (2002–2009) has produced a similar number of positive and negative events, thus covering the whole period fairly evenly (Fig. 2a). Moreover, this relationship is consistent over the whole year, although anomalies associated with the SAM are substantially larger in winter, when layers are deeper, than in summer (approximately ±50 m variability during positive or negative SAM in summer and ±150 m in winter).

Many recent studies have pointed out the importance of the El Niño–Southern Oscillation (ENSO) climate variability to the Southern-Hemisphere climate[9,15,24,25]. Therefore, a similar analysis was made to investigate the effect of ENSO on the MLD. However, ENSO is associated with longer timescales, so fewer events fall in the period 2002–2009 (~2 of each polarity; see Fig. 2b). No significant results could be extracted at this time.

Forcing mechanisms

The response of the Southern Ocean to the SAM has been widely investigated[7–9,14]. Owing to the paucity of data, studies examining the mixed layer or the interior structure of the ocean have mainly drawn on the results of models. These studies have generally shown a zonal response of the MLD to the SAM, driven by zonally symmetric Ekman pumping anomalies and Ekman heat transport due to a strengthening of the westerly winds. In contrast, our observations indicate a strongly non-zonal response of the MLD to the SAM.

To determine the physical mechanism driving the non-zonal response, we examined the air–sea heat-flux pattern associated with the SAM (Fig. 3). As expected, the Ekman heat-flux anomaly

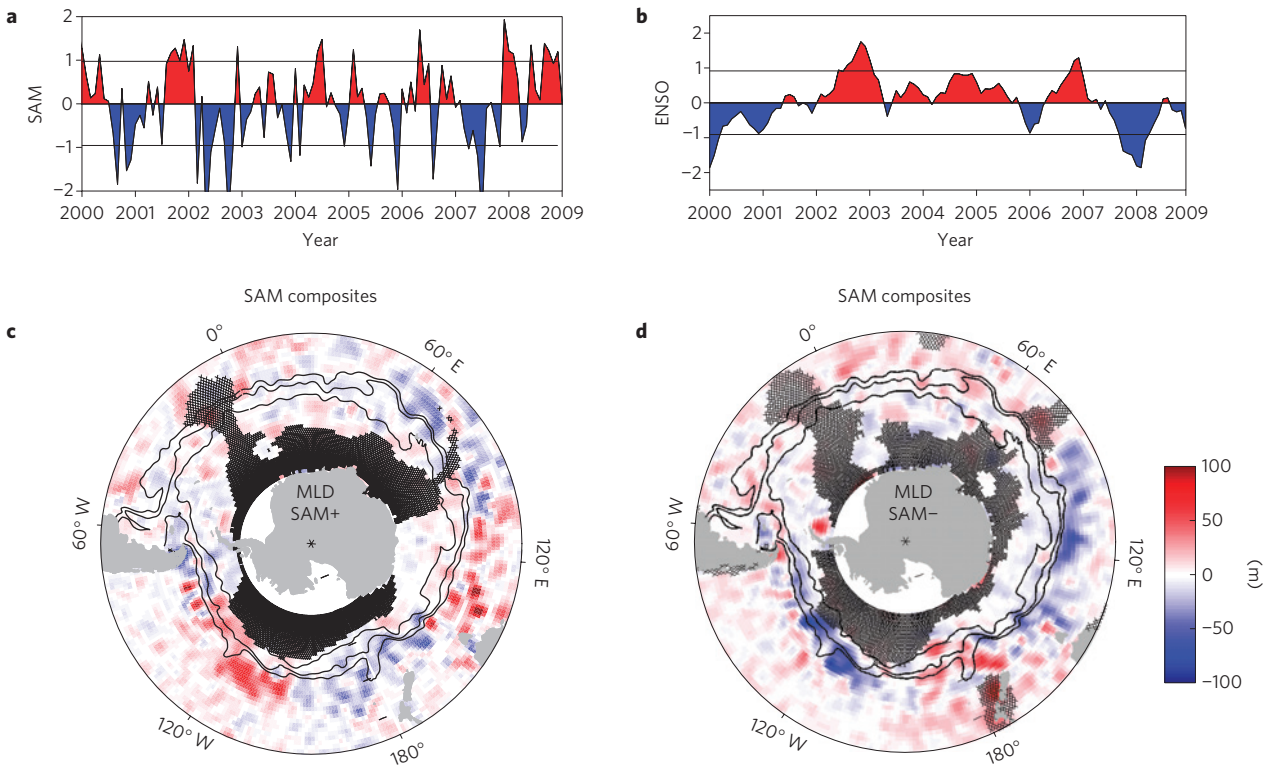

Figure 2 | MLD anomaly associated with the SAM. a,**b**, Time-series of SAM (**a**) and ENSO (**b**). The black horizontal lines show the value of the ±one standard deviation for each index. **c**,**d**, The mapped composite of the MLD anomaly during positive (**c**) and negative (**d**) SAM events from Argo data. The cross-hatching indicates bins with mapping radius greater than 800 km. The black lines show the mean positions of the three main ACC fronts[9].

associated with the SAM is indeed almost zonal (Fig. 3a,b). However, air–sea heat-flux anomalies (departure from the climatological seasonal cycle) associated with the SAM show a strongly non-zonal distribution, with a pattern similar to the MLD anomaly (Fig. 3a). Regression of the heat-flux anomaly onto the SAM shows that this pattern is associated with anomalous negative heat fluxes of about $-20\,W\,m^{-2}$ over the eastern Indian basin (100°–140° E) and over the central Pacific basin (100°–140° W) and a positive anomaly around $20\,W\,m^{-2}$ in the western Pacific basin (140° E–140° W). This pattern persists over a suite of commonly used heat-flux products (JRA-25, NCEP2 and objectively analysed air–sea fluxes OAFlux). Such a pattern has also been found in models[11,12,15], and explained by meridional wind anomalies associated with the SAM, with northward anomalous flow bringing cold air over the central Pacific and the eastern Indian oceans (Fig. 3a). Indeed, the sea-level pressure regression onto the SAM reveals a zonal structure of the SAM at lower latitudes, with one small deviation south of Tasmania (140° E) and one large intrusion of low pressure in the eastern Pacific (see Fig. 3a). This small non-zonality has a large impact on meridional winds, which greatly affect the air temperature and therefore the air–sea fluxes. The Ekman heat-transport anomaly during a positive SAM event cools the mixed layer south of the ACC and warms it north of fronts, except in the eastern Indian Ocean, south of Tasmania, and the eastern Pacific Ocean, where the Ekman heat anomaly cools the mixed layer north of the fronts (Fig. 3b). Although Ekman and air–sea heat fluxes have similar patterns, the intensity of the flux is largely dominated by air–sea flux anomalies (Fig. 3c).

Such air–sea flux anomalies are likely to be associated with an MLD anomaly. Atmospheric anomalies can influence the MLD through increased wind stress, which deepens the surface layer by mechanical stirring, or through buoyancy fluxes[26]. Simple scaling analysis shows that in the deep mixed layers north of the ACC wind stirring is negligible, and the buoyancy forcing dominates by an order of magnitude. In an attempt to estimate the expected MLD anomaly from the observed heat forcing, we approximate the buoyancy forcing from its heat component. The heat forcing in the Southern Ocean mixed layer is dominated by air–sea heat-flux forcing and Ekman transport[27,28]. Therefore, we estimate the expected MLD anomaly induced by the SAM through a simplified mixed-layer heat budget forced by the air–sea heat-flux anomalies and Ekman heat fluxes regressed onto the SAM (see the Methods section). Figure 4b shows the expected MLD anomaly during a positive SAM event. We find a deepening of the mixed layer in the eastern Indian (110°–140° E) and central Pacific (90°–140° W) oceans of the order of 100 m, with shallowing in the western Pacific (170° E–140° W) and in the central Indian (50°–110° E) oceans. Composites presented in Fig. 2 mix SAM events of different intensities and are therefore not directly comparable. Figure 4a shows a composite of the MLD anomaly weighted with the corresponding SAM event intensity for each profile, thereby wrapping positive and negative SAM events into a single map comparable to a regression of the MLD onto the SAM. The observed MLD anomaly during SAM events is in very good agreement with the expected deepening from surface heat forcing. Both the pattern and size of the MLD anomaly observed from Argo floats are well explained to first order by this simplified heat budget (Fig. 3).

The MLD anomaly due to surface forcing is associated with a mixed-layer temperature anomaly through the simplified heat budget. This gives us the opportunity to test our results, because remote-sensing products provide us with a good estimate of the surface-temperature anomaly regressed onto the SAM (see Fig. 4c). Once again, we find that the simplified heat budget produces a temperature anomaly comparable to the observed anomaly associated with the SAM. This is consistent with previous studies

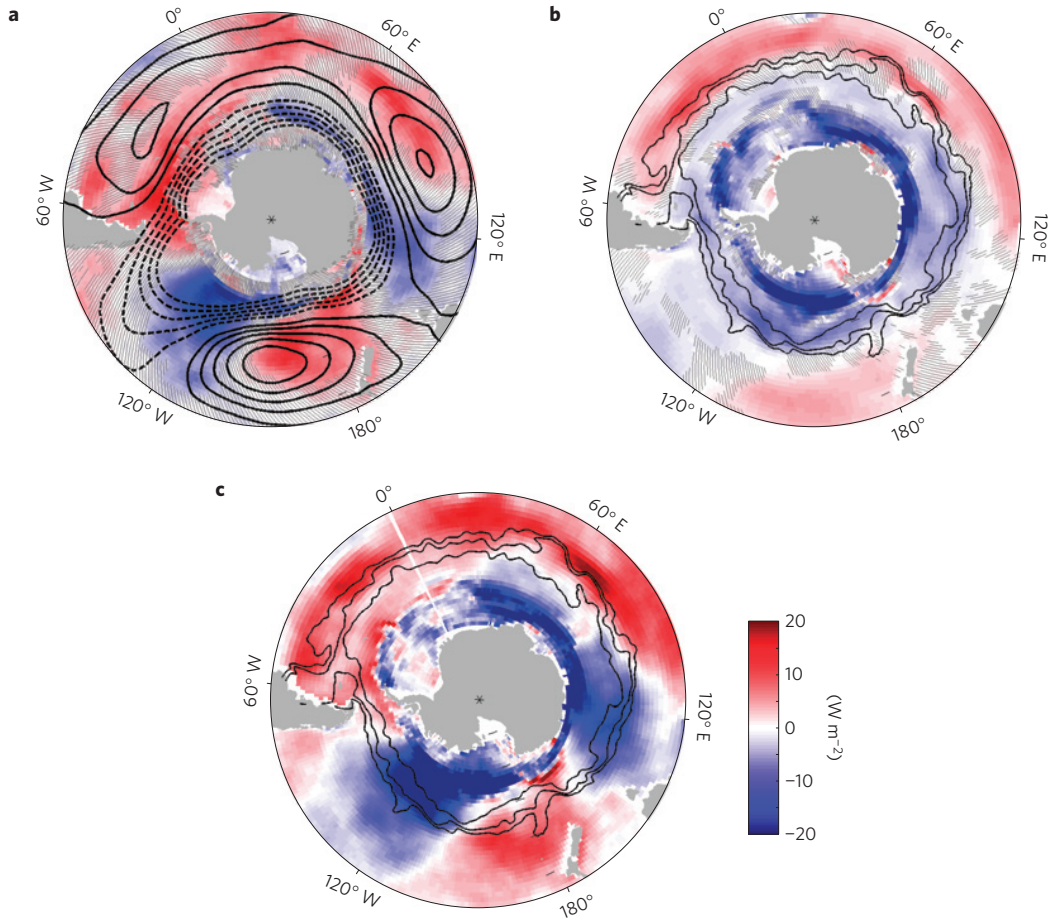

Figure 3 | Mixed-layer heat forcing associated with the SAM. a, Net air–sea heat flux from the JRA-25 reanalysis (colour) and sea-level pressure (black lines) regressed onto the SAM. **b**, Ekman heat fluxes from JRA-25 regressed onto the SAM. **c**, Sum of Ekman and air–sea heat fluxes regressed onto the SAM. Positive values refer to the ocean gaining heat. Non-significant values are cross-hatched in **a** and **b**. The black lines show the mean positions of the three main ACC fronts[9].

showing that the large-scale Southern Ocean surface-temperature anomaly is set to first order by air–sea flux anomalies[10–12].

The effect of changes in mixed-layer depth on productivity

The relationship between MLD and phytoplankton concentration is complex. The MLD affects both the phytoplankton growth[14,29] (for example, nutrient concentration and light availability) and the phytoplankton grazing (for example, zooplankton concentration). The effect of MLD on phytoplankton concentration can be immediate or lagged in time. For example, the nutrient concentrations essential to phytoplankton growth are more likely set by the winter maximum mixed layer than the summer MLD (ref. 30), whereas the light availability in the summer directly affects phytoplankton growth during this period. However, even this summer relationship between MLD and phytoplankton biomass is complex and nonlinear. For example, deepening of a mixed layer that is already very deep may have little impact on light availability, whereas small changes in depth of a mixed layer entirely exposed to sunlight may cause significant changes in phytoplankton growth rates. The depth of the mixed layer relative to the nutricline will determine the nutrient supply resulting from a change in MLD, in a similar way[30]. Here we investigate whether, despite these complicating factors, there is evidence of a relationship between changes in summer MLD and summer phytoplankton concentrations.

Previous studies have inferred a relationship between MLD changes and phytoplankton activity[14,29]. However, these studies assumed that the MLD anomaly was determined by the anomalous vertical Ekman pumping and was therefore largely zonal[14]. Our results indicate that this assumption is incorrect and therefore we reassess the connection between MLD variations driven by SAM events and surface phytoplankton biomass inferred from satellite ocean-colour data. Figure 4 shows the relationship between anomalies in surface chlorophyll concentration and MLD during positive SAM events in summer (November–February) for three regions, in places where large MLD anomalies are observed (that is, in the Subantartic Zone): the southeast Indian Ocean (110°–140° E), the southwest Pacific Ocean (140–180° W) and the central Pacific Ocean (110°–140° W).

In all three regions, an increase in MLD results in a decrease in chlorophyll concentration. In the southeast Indian Ocean and central Pacific, a 50 m increase in MLD is associated with a reduction in surface chlorophyll concentration of 0.021 mg m^{-3} and 0.013 mg m^{-3}, respectively (linear regressions significant at the 99% level; Fig. 5a,c). The relationship in the southwest Pacific is of the same sign but is not statistically significant. We note that the relationships found here between chlorophyll concentrations and SAM are two to three times larger than in previous work that did not consider variations in the MLD (ref. 14). The results are consistent with the hypothesis that the availability of light for phytoplankton growth in the Subantartic Zone is directly reduced by increases in MLD associated with positive summer SAM events. Although we consider only light availability in this study, we note that dilution of chlorophyll and physiological adaptation

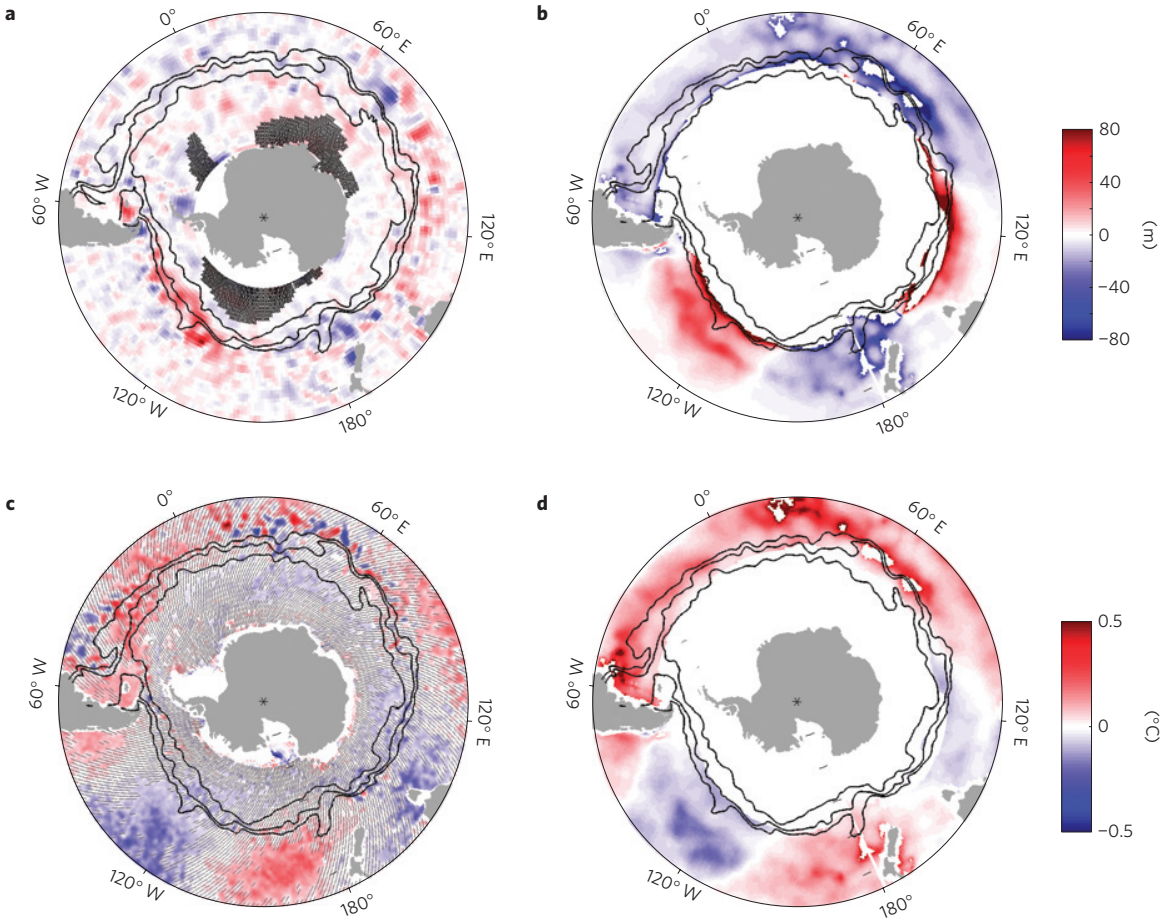

Figure 4 | Observed and expected MLD and temperature anomaly during a SAM event. a, Composite of MLD anomaly weighted with the corresponding SAM event intensity for each profile, providing a map comparable to a regression of the MLD onto the SAM. Cross-hatching indicates bins with mapping radius greater than 800 km. **b**, Expected deepening during a positive SAM event from JRA air–sea and Ekman heat fluxes regressed onto the SAM, and observed stratification at the base of the mixed layer from Argo. **c**, Observed surface temperature regressed onto the SAM. **d**, Expected temperature change associated with the expected MLD anomaly in **b**. The black lines show the mean positions of the three main ACC fronts[9].

of phytoplankton could also modulate chlorophyll concentration when MLD is changed. The respective role of each of these processes is left for future investigations.

Consequences of variations in mixed-layer depth

Meridional wind anomalies associated with departures of the SAM from zonal symmetry advect air masses across the SST gradient and alter the air–sea flux of heat. These anomalous air–sea heat fluxes drive a zonally asymmetric response of the MLD to the SAM. As variations in MLD can affect a wide range of physical, biological and biogeochemical properties of the ocean, the demonstrated link between the SAM and MLD has widespread implications.

Changes in depth of the mixed layer influence both the properties and subduction rate of water masses. For example, entrainment of fluid by a deepening mixed layer will alter the temperature, salinity, nutrient and dissolved gas concentrations of the mixed layer. The lateral advection of water in regions where the horizontal gradient of MLD is large results in subduction of surface waters into the ocean interior[16,31]. MLD variations associated with the SAM are therefore likely to have important consequences for the ventilation of the thermocline and the rate of heat and carbon storage by the ocean. Experiments with an idealized model showed that variations in MLD were the main regulator of the air–sea exchange of oxygen and carbon dioxide[15]. Changes in the mixed layer also influence the availability of light and nutrients, and therefore the rate of phytoplankton growth in the Southern Ocean is also linked to the SAM (Fig. 5). As primary production is linked to the carbon cycle, SAM-driven changes in MLD and productivity may initiate feedbacks that enhance or reduce trends in climate[22].

The SAM has experienced a significant trend towards its positive phase in recent decades, resulting in strengthening and poleward shift of the westerly winds[32]. The increase in the SAM index over the past 50 years is approximately equal to one standard deviation. Our results indicate that such a change in the SAM should have caused changes in MLD of roughly 50–100 m in the areas of deepest mixed layers. The SAM trend is largest in the summer months[32], suggesting that a SAM-forced change in MLD would be more pronounced in summer, the period of largest phytoplankton growth.

Given the influence of the mixed layer on the carbon cycle and heat storage by the ocean, it is critical that climate models can represent the mean state and variability of the mixed layer. However, the current class of Intergovernmental Panel on Climate Change models vary widely in their ability to reproduce the observed mean depth of the mixed layer and its seasonal cycle[33]. Models that fail to reproduce the mean state of the Southern Ocean mixed layer are unlikely to do a good job of simulating anomalies in MLD. Indeed, a recent coarse-resolution coupled climate model thought to be representative of the state of the art does not capture the observed zonally asymmetric response of the MLD to the SAM (ref. 8). This raises concerns that the current generation of models may not yet adequately capture the interaction between the ocean and atmosphere, as mediated through the surface mixed layer.

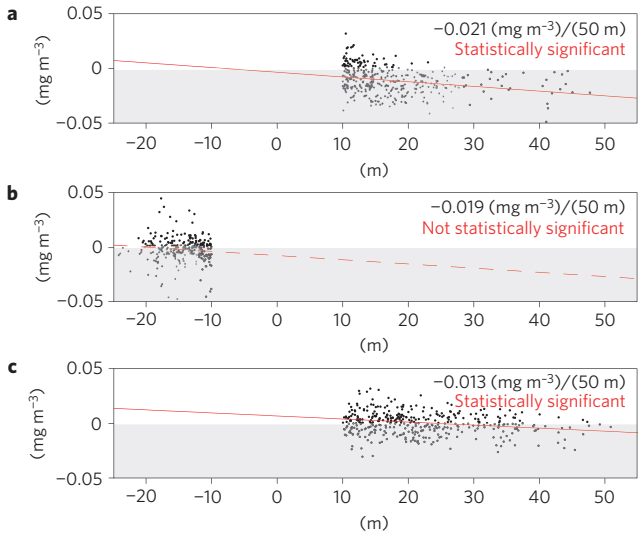

Figure 5 | Averaged summer chlorophyll-concentration response to MLD anomaly. a–c, Chlorophyll-concentration anomaly during a SAM event versus MLD anomaly associated with a SAM event. Three regions where we observe MLD anomalies above 10 m (that is, regions of the Subantartic Zone) are shown: the southeastern Indian sector (110°–140°E) (**a**), the southwestern Pacific basin (140°–180° W) (**b**) and the central Pacific basin (110°–140° W) (**c**).

Our observations and physical explanation for a response of the Southern Ocean mixed layer to the SAM provide a target for future model improvements.

Methods

In this study, we map information from Argo profiles using a loess fitting method[34]. At each grid point, this method searches for the closest points within a radius of 200 km, then the radius gradually increases until it encloses at least 100 points. We set the method to not be able grow its radius above 1,500 km. The profiles found within the final radius size are mapped at the grid point using a loess method. We chose to use such a method primarily because it does not require a first-guess estimate, as does an optimal interpolation algorithm. Both radius size and standard error enable us to assess the accuracy of the resulting field (see Supplementary Information).

MLD, mixed-layer temperature and stratification at the base of the mixed layer were extracted from the Argo dataset (www.argo.ucsd.edu). We calculated the MLD for every Southern Ocean profile with a surface-density-difference criterion[23,35] of $\Delta\sigma \leq 0.03\,\mathrm{kg\,m^{-3}}$ and mapped monthly averages by a loess fitting method. The extensive coverage provided by the Argo dataset enabled us to obtain monthly maps of MLD on half-degree grids with error estimates. We also produced a database of MLD anomalies from the seasonal cycle, from which composite databases of MLD anomalies during positive and negative SAM events were extracted and gridded with a loess fitting method.

The monthly SAM index and the ENSO index were obtained from the NOAA Climate Prediction Center website (http://www.cdc.noaa.gov) for the period 1979–2008. The SAM index is defined as the first principal component of monthly 700 hPa geopotential height anomalies from the NCEP-NCAR reanalysis dataset. We also used the Nino3.4 ENSO index. Its variations are based on SST anomalies averaged over the region spanning 5° N–5° S, 170°–120° W.

To estimate the air–sea heat-flux anomaly associated with a SAM event, we use the JRA-25 reanalysis data (http://jra.kishou.go.jp). This recent reanalysis is expected to be more realistic because it includes more observational data than the other products[36]. To match the Argo period, we regressed anomalies of the field from this product over the period 2002–2008. Anomalies in this study are defined as a deviation from the climatological seasonal cycle. The integrated Ekman heat flux in the Ekman layer was computed using winds (τ) and SST field: Ekman flux $= \rho C_p(\mathbf{U_E}\nabla\mathrm{SST})$; where ρ is the density of the water, C_p is the specific heat capacity, ∇ is the gradient operator and $\mathbf{U_E} = (1/\rho f)(\tau^y, \tau^x)$ is the Ekman transport.

We also compared the regressed fields of heat fluxes onto the SAM with those from NCEP-2 (http://www.cdc.noaa.gov) and the OAFlux (objectively analysed air–sea fluxes). All three regressions produced very similar results, the collocated standard deviation of the three regressions ranging from 0 to $10\,\mathrm{W\,m^{-2}}$ with an average standard deviation over the area studied here (−60°/−35° S) of only $2\,\mathrm{W\,m^{-2}}$.

Surface temperature is from the global satellite SST product from TMI and AMSR satellites (http://www.ssmi.com/). As the area studied is mainly outside the boundary of the TMI satellite, most of the data are from the AMSR-E satellite. A comparison of AMSR-E SSTs with expendable bathythermograph (XBT) repeated sections shows that the standard error is less than 0.1°C during winter[37].

Finally, we estimate the chlorophyll concentration in the surface waters from the data provided by the SEAWIFS Project, NASA Goddard Space Flight Center and GeoEye.

Expected MLD and temperature anomalies were estimated from heat-flux forcing anomalies and the climatological stratification below the mixed layer. We considered the heat budget: $\partial T/\partial t = Q/(H\rho C_p)$, where H, T and ρ are, respectively, the MLD, temperature and density; Q is the heat forcing and C_p is the specific heat capacity. From this equation, we could estimate the anomaly H' of MLD created by a heat-forcing anomaly δQ applied over a time Δt. To do so, we assume that the MLD anomaly H' and temperature anomaly T' follow the slope of the climatological stratification at the base of the mixed layer: $[\partial T/\partial z]_{\mathrm{baseML}} = T'/H'$, which is computed from the Argo array.

Received 16 September 2009; accepted 3 February 2010; published online 14 March 2010

References

1. Thompson, D. & Wallace, J. Annular mode in the extratropical circulation. Part I: Month-to-month variability. *J. Clim.* **13,** 1000–1016 (2000).
2. Thompson, D. & Solomon, S. Interpretation of recent Southern Hemisphere climate change. *Science* **296,** 895–899 (2002).
3. Yin, J. H. A consistent poleward shift of the storm tracks in simulations of 21st century climate. *Geophys. Res. Lett.* **32,** L18701 (2005).
4. Russell, J. L., Dixon, K. W., Gnanadesikan, A., Stouffer, R. J. & Toggweiler, J. R. The Southern Hemisphere westerlies in a warming world: Propping open the door to the deep ocean. *J. Clim.* **19,** 6382–6390 (2006).
5. Stammerjohn, S. E., Martinson, D. G., Smith, R. C., Yuan, X. & Rind, S. Trends in Antarctic annual sea ice retreat and advance and their relation to ENSO and Southern Annular Mode variability. *J. Geophys. Res.* **113,** C03S90 (2008).
6. Meredith, M. & Hogg, A. Circumpolar response of the Southern Ocean eddy activity to changes in the Southern Annular Mode. *Geophys. Res. Lett.* **33,** L16608 (2006).
7. Hall, A. & Visbeck, M. Synchronous variability in the Southern Hemisphere atmosphere, sea ice, and ocean resulting from the annular mode. *J. Clim.* **15,** 3043–3057 (2002).
8. Sen Gupta, A. & England, M. Coupled ocean–atmopshere–ice response to variations in the Southern Annular Mode. *J. Clim.* **19,** 4457–4486 (2006).
9. Sallée, J. B., Morrow, R. & Speer, K. Response of the Antarctic Circumpolar Current to atmospheric variability. *J. Clim.* **21,** 3020–3039 (2008).
10. Ciasto, L. & Thompson, D. Observations of large-scale ocean–atmosphere interaction in the Southern Hemisphere. *J. Clim.* **21,** 1244–1259 (2008).
11. Verdy, A., Marshall, J. & Czaja, A. Sea surface temperature variability along the path of the Antarctic Circumpolar Current. *J. Phys. Oceanogr.* **36,** 1317–1331 (2006).
12. Vivier, F., Iudicone, D., Busdraghi, F. & Park, Y.-H. Dynamics of sea surface temperature anomalies in the Southern Ocean diagnosed from a 2-D mixed-layer model. *Clim. Dynam.* **34,** 153–184 (2009).
13. Le Quéré, C. *et al.* Saturation of the Southern Ocean CO_2 sink due to recent climate change. *Science* **316,** 1735–1738 (2007).
14. Lovenduski, N. & Gruber, N. Impact of the Southern Annular Mode on the Southern Ocean circulation and biology. *Geophys. Res. Lett.* **32,** 1–4 (2005).
15. Verdy, A., Dutkiewicz, S., Follows, M., Marshall, J. & Czaja, A. Carbon dioxide and oxygen fluxes in the Southern Ocean: Mechanisms of interannual variability. *Glob. Biogeochem. Cycles* **21,** GB2020 (2007).
16. Sallée, J. B., Speer, K., Rintoul, S. & Wijffels, S. Southern Ocean thermocline ventilation. *J. Phys. Oceanogr.* **40,** 509–529 (2010).
17. McCartney, M. *Subantarctic Mode Water* (Pergamon Press, 1977).
18. Sloyan, B. & Rintoul, S. Circulation, renewal and modification of Antarctic Mode Water and Intermediate Water. *J. Phys. Oceanogr.* **31,** 1005–1030 (2001).
19. Rintoul, S., Hughes, C. & Olbers, D. *The Antarctic Circumpolar Curent System* 271–302 (Academic, 2001).
20. Sarmiento, J., Gruber, N., Brzezinski, M. & Dunne, J. High-latitude controls of thermocline nutrients and low latitude biological productivity. *Nature* **427,** 56–60 (2004).
21. Sabine, C. *et al.* The oceanic sink for anthropogenic CO_2. *Science* **305,** 367–371 (2004).
22. Boyd, P. & Doney, S. C. *Ocean Biogeochemistry* 157–193 (Springer, 2003).
23. Dong, S., Sprintall, J., Gille, S. & Talley, L. Southern Ocean mixed-layer depth from Argo float profiles. *J. Geophys. Res.* **113,** C06013 (2008).
24. Karoly, D. Southern Hemisphere circulation features associated with El-Nino–Southern Oscillation events. *J. Clim.* **2,** 1239–1252 (1989).
25. Fogt, R. & Bromwich, D. Decadal variability of the ENSO teleconnection to the high latitude South Pacific governed by coupling with the Southern Annular Mode. *J. Clim.* **19,** 979–997 (2006).

26. Kraus, E. B. & Turner, J. S. A one-dimensional model of the seasonal thermocline. *Tellus* **19,** 88–97 (1966).
27. Rintoul, S. & England, M. Ekman transport dominates air–sea fluxes in driving variability of Subantarctic Mode Water. *J. Phys. Oceanogr.* **32,** 1308–1321 (2002).
28. Dong, S., Sprintall, J. & Gille, S. An assessment of the Southern Ocean mixed layer heat budget. *J. Clim.* **20,** 4425–4442 (2007).
29. Boyd, P. P. W. *et al.* Climate-mediated changes to mixed-layer properties in the Southern Ocean: Assessing the phytoplankton response. *Biogeosciences* **5,** 847–864 (2008).
30. Boyd, P. *et al.* A mesoscale phytoplankton bloom in the polar Southern Ocean stimulated by iron fertilization. *Nature* **407,** 695–702 (2000).
31. Huang, R. X. The three-dimensional structure of wind-driven gyres: Ventilation and subduction. *Rev. Geophys.* **29** (suppl.), 590–609 (1991).
32. Marshall, G. Trends in the Southern Annular Mode from observations and reanalyses. *J. Clim.* **16,** 4134–4143 (2003).
33. Downes, S., Bindoff, N. & Rintoul, S. Impact of climate change on the subduction of mode and intermediate water masses in the Southern Ocean. *J. Clim.* **22,** 3289–3302 (2009).
34. Ridgway, K., Dunn, J. & Wilkin, J. Ocean interpolation by four-dimensional weighted least squares: application to the waters around Australasia. *J. Atmos. Ocean. Technol.* **19,** 1357–1375 (2002).
35. Sallée, J. B., Wienders, N., Morrow, R. & Speer, K. Formation of Subantarctic Mode Water in the southeastern Indian Ocean. *Ocean Dyn.* **56,** 525–542 (2006).
36. Onogi, K. *et al.* The JRA-25 reanalysis. *J. Meteorol. Soc. Jpn* **85,** 369–432 (2007).
37. Dong, S., Sprintall, J. & Gille, S. Location of the Polar Front from AMSR-E satellite sea-surface temperature measurements. *J. Phys. Oceanogr.* **36,** 2075–2089 (2006).

Acknowledgements

We acknowledge the role of Jeff Dunn in developing and making available the loess fitting method. K.G.S. received support from NSF OCE-0822075, OCE-0612167 and OCE-0622670. J.B.S. was supported by a CSIRO Office of the Chief Executive (OCE) postdoctoral fellowship. S.R.R. was supported by the Australian Government's Cooperative Research Centres Programme through the Antarctic Climate and Ecosystems Cooperative Research Centre (ACE-CRC). J.B.S. and S.R.R. were also supported by the CSIRO Wealth from Oceans National Research Flagship. This study has benefited from discussions with R. Matear, A. Lenton, N. Cassar and P. Boyd.

Author contributions

J.B.S. directed the analysis of the several datasets used in this study and shared responsibility for writing the manuscript. K.G.S. and S.R.R. participated in the data analysis and shared responsibility for writing the manuscript. All authors contributed to the final version of the manuscript.

Additional information

The authors declare no competing financial interests. Supplementary information accompanies this paper on www.nature.com/naturegeoscience. Reprints and permissions information is available online at http://npg.nature.com/reprintsandpermissions. Correspondence and requests for materials should be addressed to J.B.S.